

Quantum correlations close to a square pattern forming instability

M. Hoyuelos¹, G.-L. Oppo², P. Colet^{3,a}, and M. San Miguel³

¹ Departamento de Física, Facultad de Ciencias Exactas y Naturales, Universidad Nacional de Mar del Plata, Funes 3350, 7600 Mar del Plata, Argentina

² Department of Physics, University of Strathclyde, John Anderson Building, 107 Rottenrow, Glasgow G4 0NG, UK

³ Instituto Mediterráneo de Estudios Avanzados^b, IMEDEA (CSIC-UIB), Campus Universitat Illes Balears, 07071 Palma de Mallorca, Spain

Received 17 September 2002 / Received in final form 11 November 2002

Published online 26 February 2003 – © EDP Sciences, Società Italiana di Fisica, Springer-Verlag 2003

Abstract. We analyze the quantum fluctuations of the degenerate optical parametric oscillator close to an instability for the formation of a square pattern. While strong correlations between the fluctuations of the signal modes emitted at the critical wave number and with opposite wave vector are present both below and above threshold, no features signaling the square character of the pattern forming above threshold have been identified below threshold in the spatio-temporal second-order coherence. We also explore in which regimes a reduced few mode model gives meaningful results.

PACS. 42.50.Lc Quantum fluctuations, quantum noise, and quantum jumps – 42.65.Sf Dynamics of nonlinear optical systems; optical instabilities, optical chaos and complexity, and optical spatio-temporal dynamics

1 Introduction

Patterns in extended nonlinear optical systems have the interesting feature of displaying noteworthy quantum aspects at room temperature, which is often not the case with more traditional fields associated with spontaneous spatial structures such as hydrodynamics, chemical reactions or biology. These quantum aspects, which arise from the quantum correlation of the spatial modes that form the pattern, have attracted the interest of researchers during the last years (see for example [1–14] and Ref. [15] for a review on optical pattern formation and its quantum fluctuations). For example, quantum features are found both below and above the instability threshold for pattern formation in optical parametric oscillators (OPO). In particular it has been shown that below, but close to, threshold, the quantum noise can excite the weakly damped spatial modes that will become unstable at threshold [1–3]. In an isotropic system with two spatial dimensions, the spectrum of fluctuations below threshold has a radially symmetric distribution with maxima on a ring of radius equal to the wave-number of the pattern formed just above threshold. Therefore, the spectrum of fluctuations below the instability threshold is considered to be a noisy precursor [16] that anticipates the above-threshold pattern wave-

number. Furthermore, in optical systems where a stripe pattern is formed, strong correlations exist, even at quantum level, between the fluctuations in the number of photons emitted at the critical wave-number ($|\mathbf{k}| = k_c$) and opposite wave-vectors. This is an effect of the parametric coupling associated with transverse momentum conservation. It has been interpreted as a below-threshold signal of the form of the pattern that will arise above threshold, namely a stripe pattern. The fact that the correlations are associated with quantum entanglement among spatial modes has originated the term “quantum image” [1].

The most common pattern to appear above threshold in a degenerate OPO (DOPO) is a stripe pattern [17] with a far field formed by two off axis beams. These beams correspond to the simultaneous emission of twin photons with a high degree of quantum correlation of their fluctuations. High above threshold a spatially disordered structure emerges in which k_c plays no particular role. Still, strong quantum correlations between pair of opposite wavevectors persist in a one dimensional geometry [18]. In the non-degenerate OPO quantum correlations are also found between the off axis emissions of the signal and idler field modes [9].

A semi-classical analysis of pattern formation in the DOPO [19,20] shows that for specific values of the cavity detuning parameters, a square pattern, instead of a roll pattern, emerges. In this paper we study the quantum

^a e-mail: pere@imedea.uib.es

^b <http://www.imedea.uib.es/PhysDept/>

fluctuations and correlations at the onset of the instability that leads to the formation of a square pattern in a degenerate OPO. In particular we investigate whether below threshold there is any correlation in the fluctuations of the far field modes with different transverse wave vectors that can be interpreted as an anticipation of the square pattern that appears above threshold. Since we are interested in calculating field intensity correlation between two different space-time points, the appropriate quantity to be used is the second order quantum correlation function g_2 (see, for example, Ref. [22]).

We show that, below threshold, the g_2 function indicates strong correlations between the fluctuations of the signal critical modes with opposite wave vectors, as in the case of stripe pattern formation. However in a continuous model and within our rather high numerical accuracy, no correlation is found below threshold between the fluctuations of signal critical modes with wave vectors forming an angle of $\pi/2$. These $\pi/2$ -angle correlations are present above threshold, as a consequence of the square form of the pattern. Its presence below threshold could have been interpreted as a quantum image of the square pattern to emerge after the onset of the instability. Therefore below threshold the spectrum of fluctuations provides information about the pattern wave number (noisy precursor in the classical sense) but does not seem to reveal or anticipate the square shape which will be formed above threshold. Furthermore, particular caution has to be taken when interpreting g_2 measurements in a truncated model obtained by projecting the stochastic dynamics on just 4 modes corresponding to the square components. While this model gives meaningful results for the dynamics above threshold, its results below threshold are not valid. In particular, we show that very close but still below threshold $\pi/2$ -angle anti-correlations in the g_2 exist for this projected model. This apparently spurious result is due to the mode-truncation and disappears moving further below threshold and in the continuous limit.

The article is organized as follows. In Section 2 we introduce the continuous model used for the description of the quantum DOPO dynamics. In Section 3 we define the correlation function g_2 in a way appropriate for the numerical calculations. In Section 4 we show the results of the numerical integration of the continuous model. In Section 5 we introduce a truncated model with the minimal number of modes to describe the square pattern. Section 6 is devoted to concluding remarks. Finally, in the Appendix we explain the procedure we use to calculate numerically the output field.

2 The model

We use the space dependent quantum Langevin equations for the DOPO obtained in reference [3]. The system consists in a $\chi^{(2)}$ medium enclosed in a single port cavity with plane mirrors pumped by a coherent, monochromatic field of frequency 2ω . The pump power is partially converted from the pump frequency (2ω) to the signal frequency ω .

The intracavity pump and signal fields are described by the space-time dependent quantum operators $A_0(\mathbf{x}, t)$ and $A_1(\mathbf{x}, t)$ respectively, where \mathbf{x} represents a point in the plane perpendicular to the direction of light propagation.

The Hamiltonian in the interaction picture is

$$H = H_f + H_{\text{int}} + H_{\text{ext}} \quad (1)$$

where the free propagation of the fields, including diffraction effects, is represented by

$$H_f = \hbar\gamma_0 \int d\mathbf{x} A_0^\dagger (\Delta_0 - a_0 \nabla^2) A_0 + \hbar\gamma_1 \int d\mathbf{x} A_1^\dagger (\Delta_1 - a_1 \nabla^2) A_1. \quad (2)$$

The constants γ_0 and γ_1 are the cavity damping rates for the two fields; $\Delta_0 = (\omega_{c0} - 2\omega)/\gamma_0$ and $\Delta_1 = (\omega_{c1} - \omega)/\gamma_1$ are the cavity detuning parameters (ω_{c0} and ω_{c1} are the frequencies of the two longitudinal cavity modes closest to 2ω and ω). Parameters a_0 and a_1 are characteristic areas that represent the strength of diffraction; and ∇^2 is the two dimensional transverse Laplacian which models the effect of diffraction in the paraxial approximation.

The term H_{int} in equation (1) represents the nonlinear interaction Hamiltonian

$$H_{\text{int}} = \frac{i\hbar g}{2} \int d\mathbf{x} \left(A_0 A_1^{\dagger 2} - A_0^\dagger A_1^2 \right), \quad (3)$$

where g is the coupling parameter related to the nonlinearity of the medium. The third term in equation (1) represents the coherent and monochromatic external driving

$$H_{\text{ext}} = i\hbar \int d\mathbf{x} \left(E_{\text{in}} A_0^\dagger - E_{\text{in}}^* A_0 \right), \quad (4)$$

where E_{in} is the (scaled) plane wave pump field amplitude.

The reversible part of the dynamics is represented by the Hamiltonian. The irreversible part is introduced in the Liouvillian terms of the master equation for the density matrix. The master equation can be turned into a set of stochastic differential equations for c -number fields $\alpha_0(\mathbf{x}, t)$ and $\alpha_1(\mathbf{x}, t)$ corresponding to the operators $A_0(\mathbf{x}, t)$ and $A_1(\mathbf{x}, t)$, in the Wigner representation [3, 4, 15, 21]. The nonlinear Langevin equations are

$$\frac{\partial \alpha_0}{\partial t} = -\gamma_0 (1 + i\Delta_0 - ia_0 \nabla^2) \alpha_0 + E_{\text{in}} - g\alpha_1^2/2 + \sqrt{2\gamma_0} \xi_0 \quad (5)$$

$$\frac{\partial \alpha_1}{\partial t} = -\gamma_1 (1 + i\Delta_1 - ia_1 \nabla^2) \alpha_1 + g\alpha_0\alpha_1^* + \sqrt{2\gamma_1} \xi_1. \quad (6)$$

Variables ξ_0 and ξ_1 are white noise stochastic Gaussian processes with zero average, and correlation

$$\langle \xi_i(\mathbf{x}, t) \xi_i^*(\mathbf{x}', t') \rangle = \frac{1}{2} \delta(\mathbf{x} - \mathbf{x}') \delta(t - t')$$

for $i = 0, 1$. The noise terms are interpreted as vacuum quantum noise entering through the partially transmitting mirror.

Equations (5, 6) can be numerically integrated to calculate symmetrically ordered correlations as

$$\langle A_1^\dagger(\mathbf{x}, t) A_1(\mathbf{x}', t') \rangle_{\text{sym}} = \left\langle \frac{A_1^\dagger(\mathbf{x}, t) A_1(\mathbf{x}', t') + A_1(\mathbf{x}, t) A_1^\dagger(\mathbf{x}', t')}{2} \right\rangle = \langle \alpha_1^*(\mathbf{x}, t) \alpha_1(\mathbf{x}', t') \rangle. \quad (7)$$

The c -number fields outside the cavity, $\alpha_0^{\text{out}}(\mathbf{x}, t)$ and $\alpha_1^{\text{out}}(\mathbf{x}, t)$, corresponding to the operators $A_0^{\text{out}}(\mathbf{x}, t)$ and $A_1^{\text{out}}(\mathbf{x}, t)$, can be numerically calculated following the method introduced in [10]. The input-output relations

$$\alpha_i^{\text{out}} = \sqrt{2\gamma_i} \alpha_i - \alpha_i^{\text{in}} \quad (8)$$

have to be discretized in order to include noise in the numerical scheme. The input fields are

$$\alpha_0^{\text{in}} = E_{\text{in}}/\sqrt{2\gamma_0} + \xi_0; \quad \alpha_1^{\text{in}} = \xi_1. \quad (9)$$

Appendix A contains more details on the numerical implementation of the evaluation of the output fields.

Neglecting fluctuations, equations (5, 6) have a homogeneous steady state solution given by

$$\alpha_{1,s} = 0, \quad \alpha_{0,s} = \frac{E_{\text{in}}}{\gamma_0(1 + i\Delta_0)}. \quad (10)$$

This steady state homogeneous solution (10) becomes unstable as the input field is increased, and a square pattern with a critical wave number $|k_c| = \sqrt{-\Delta_1/a_1}$ appears if $\Delta_0 < -2\sqrt{3}$ [20]. The threshold value of the dimensionless input field for the instability is

$$\bar{E}_{\text{thr}} = \frac{E_{\text{thr}}}{\gamma_0 \sqrt{n_{\text{ph}}}} = \sqrt{1 + \Delta_0^2}$$

where $n_{\text{ph}} = \gamma_1^2/g^2$ represents the number of pump photons per unit area that are needed to reach the threshold for signal generation [15].

An analysis of the energy flux in the system can be useful, as we will see in Section 5, to analyze fluctuation correlations. The input and output intensities are

$$\begin{aligned} I_{\text{in}} &= \hbar 2\omega |\alpha_0^{\text{in}}|^2 + \hbar\omega |\alpha_1^{\text{in}}|^2 \\ I_{\text{out}} &= \hbar 2\omega |\alpha_0^{\text{out}}|^2 + \hbar\omega |\alpha_1^{\text{out}}|^2. \end{aligned} \quad (11)$$

Using the input-output relations (8), the net power inside the cavity is

$$\begin{aligned} P &= \int d\mathbf{x} (I_{\text{in}} - I_{\text{out}}) \\ &= 2\hbar\omega \int d\mathbf{x} [2\Re(E_{\text{in}}\alpha_0^*) - 2\gamma_0|\alpha_0|^2 - \gamma_1|\alpha_1|^2], \end{aligned} \quad (12)$$

where the terms with fluctuations ξ_i average to zero in the transverse plane. This same quantity has been used in [23] to characterise cavity soliton features in DOPO. Since P represents an average over the transverse plane of the net energy gain, its time average should be zero in any steady state. In Section 5 we use a simplified model with 4 modes to evaluate the consequences of equation (12).

3 The second order coherence function g_2

The far field of the signal outside the cavity is represented by the space Fourier transform, $A_1^{\text{out}}(\mathbf{k}, t)$. The annihilation operator of the signal field defined in a small interval of wave-vectors and time, around (\mathbf{k}_i, t_i) , is

$$\hat{a}_i = \int_{R_i} d\mathbf{k} \int_{t_i}^{t_i+\Delta t} dt \frac{A_1^{\text{out}}(\mathbf{k}, t)}{\sqrt{R\Delta t}} \quad (13)$$

where R_i is the region of integration around \mathbf{k}_i , of size R , and Δt is the time interval [24]. We consider both R and Δt independent of i . The index i represents different space-time points.

Using the commutation relation of the field outside the cavity

$$[A^{\text{out}}(\mathbf{k}, t), A^{\text{out}\dagger}(\mathbf{k}', t')] = \delta(\mathbf{k} - \mathbf{k}')\delta(t - t'), \quad (14)$$

it is easy to see that the annihilation and creation operators satisfy $[\hat{a}_i, \hat{a}_j^\dagger] = \delta_{i,j}$, where in our notation $i = j$ implies $\mathbf{k}_i = \mathbf{k}_j$ and $t_i = t_j$.

The definition of the g_2 function in terms of the creation and annihilation operators of the signal field outside the cavity is

$$g_2(\mathbf{k}_i, t_i, \mathbf{k}_j, t_j) = \frac{\langle : \hat{a}_i^\dagger \hat{a}_j^\dagger \hat{a}_j \hat{a}_i : \rangle}{\langle : \hat{a}_i^\dagger \hat{a}_i : \rangle \langle : \hat{a}_j^\dagger \hat{a}_j : \rangle}, \quad (15)$$

where $\langle :: \rangle$ represents time and normal ordering. We need to express g_2 in terms of the symmetrically ordered averages that can be obtained numerically. We briefly describe this process in the following.

First, we write g_2 in terms of continuous operators $A_1^{\text{out}}(\mathbf{k}, t)$ using equation (13). We use the commutation relation for the outside cavity field (14) to transform normally ordered averages into symmetrically ordered averages. For example, for the term in the denominator of equation (15), we have

$$\begin{aligned} \langle : \hat{a}_i^\dagger \hat{a}_i : \rangle &= \frac{1}{R\Delta t} \int_{R_i} d\mathbf{k} \int_{t_i}^{t_i+\Delta t} dt \int_{R_i} d\mathbf{k}' \\ &\quad \times \int_{t_i}^{t_i+\Delta t} dt' \langle : A_1^{\text{out}\dagger}(\mathbf{k}, t) A_1^{\text{out}}(\mathbf{k}', t') : \rangle \\ &= \frac{1}{R\Delta t} \int_{R_i} d\mathbf{k} \int_{t_i}^{t_i+\Delta t} dt \int_{R_i} d\mathbf{k}' \int_{t_i}^{t_i+\Delta t} dt' \\ &\quad \times \langle A_1^{\text{out}\dagger}(\mathbf{k}, t) A_1^{\text{out}}(\mathbf{k}', t') \rangle_{\text{sym}} - \frac{1}{2}. \end{aligned} \quad (16)$$

We can now replace the symmetrically ordered averages by the averages of the numerically calculated c -number fields, $\alpha_1^{\text{out}}(\mathbf{k}, t)$. Considering that the integration region is small, we can use the approximation $\int_{R_i} d\mathbf{k} \int_{t_i}^{t_i+\Delta t} dt \alpha_1^{\text{out}}(\mathbf{k}, t) \simeq R\Delta t \alpha_1^{\text{out}}(\mathbf{k}_i, t_i)$, and

$$\langle : \hat{a}_i^\dagger \hat{a}_i : \rangle = R\Delta t \langle |\alpha_1^{\text{out}}(\mathbf{k}_i, t_i)|^2 \rangle - 1/2. \quad (17)$$

$$g_2(\mathbf{k}_i, t_i, \mathbf{k}_j, t_j) = \frac{\langle |\alpha_{1,i}^{\text{out}}|^2 |\alpha_{1,j}^{\text{out}}|^2 \rangle - (\langle |\alpha_{1,i}^{\text{out}}|^2 \rangle + \langle |\alpha_{1,j}^{\text{out}}|^2 \rangle) (1 + \delta_{ij})/2 + (1 + \delta_{ij})/4}{(\langle |\alpha_{1,i}^{\text{out}}|^2 \rangle - 1/2) (\langle |\alpha_{1,j}^{\text{out}}|^2 \rangle - 1/2)} \quad (18)$$

After these steps we find that equation (15) can be rewritten as

see equation (18) above

where we use the dimensionless quantity $\alpha_{1,i}^{\text{out}} = \sqrt{R\Delta t} \alpha_1^{\text{out}}(\mathbf{k}_i, t_i)$ to simplify the notation. Note that if the statistics of $\alpha_{1,i}^{\text{out}}$ and $\alpha_{1,j}^{\text{out}}$ were independent then $g_2(\mathbf{k}_i, t_i, \mathbf{k}_j, t_j) = 1$, therefore a value of g_2 larger (smaller) than 1 indicates a positive correlation (anticorrelation) between $\alpha_{1,i}^{\text{out}}$ and $\alpha_{1,j}^{\text{out}}$. For equal time and position the expression reduces to

$$g_2(\mathbf{k}_i, t_i, \mathbf{k}_i, t_i) = \frac{\langle |\alpha_{1,i}^{\text{out}}|^4 \rangle - 2 \langle |\alpha_{1,i}^{\text{out}}|^2 \rangle + 1/2}{(\langle |\alpha_{1,i}^{\text{out}}|^2 \rangle - 1/2)^2}. \quad (19)$$

4 The continuous model

We study the degenerate OPO described by equations (5, 6) close to the instability that produces a square pattern. In the numerical calculations we use the parameters $\Delta_0 = -4$, $\Delta_1 = -2$, $n_{\text{ph}} = 10^6/a_1$, $2a_0 = a_1$ and $\gamma_1 = \gamma_0$. Space and time are scaled with the values of a_1 and γ_1 respectively in order to use dimensionless quantities. The numerical method of integration that we used involves a spectral integration of the diffraction part and a second order Runge-Kutta method for the rest of the equation [3].

The pump has a radially symmetric shape

$$E_{\text{in}}(r) = E_{\text{in}}^0 \left[1 + \tanh \left(\frac{r_0 - r}{w} \right) \right] / 2$$

where $r = |\mathbf{x}|$. This expression yields a large central region with a quite flat profile which decays at $r = r_0$ with a decay rate determined by w . This avoids periodic boundary condition effects. We took $r_0 = 65.5$ which is about 14.75 times the critical wavelength for pattern formation and $w = 0.667$. We define the dimensionless pump maximum amplitude as

$$\bar{E}_{\text{in}} = \frac{E_{\text{in}}^0}{\gamma_0 \sqrt{n_{\text{ph}}}}.$$

4.1 Results below threshold

Figure 1 shows an intracavity field snapshot just below threshold, for a dimensionless input field value of $\bar{E}_{\text{in}} = 4.119 = 0.999\bar{E}_{\text{thr}}$. In the near field a disordered faint pattern appears in the signal field while the intracavity

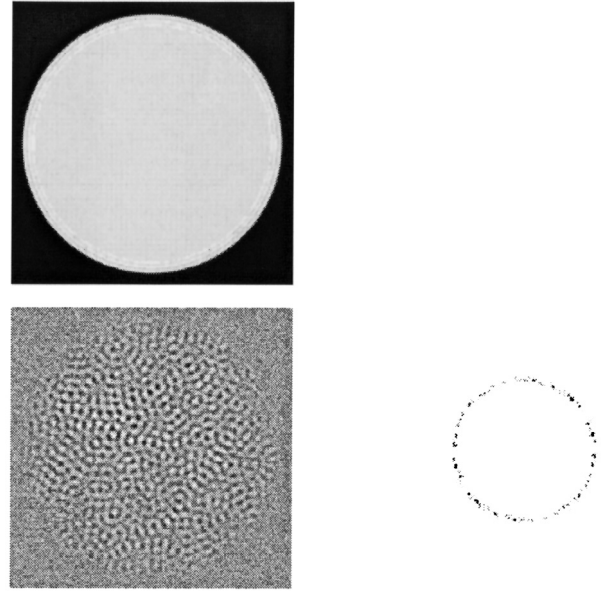


Fig. 1. Snapshot of the fields configuration just below threshold, $\bar{E}_{\text{in}} = 0.999\bar{E}_{\text{thr}}$. First row: intracavity pump near field intensity $|\alpha_0(\mathbf{x})|^2$; and far field power spectra $|\alpha_0(\mathbf{k})|^2$. Second row: real part of the intracavity signal near field $\Re(\alpha_1(\mathbf{x}))$, and far field power spectra $|\alpha_1(\mathbf{k})|^2$. The range of values for the near field configurations are $|\alpha_0(\mathbf{x})|^2 \in [0, 1.12]$ and $\Re(\alpha_1(\mathbf{x})) \in [-0.012, 0.012]$. A lattice of 256×256 points was used.

pump field remains practically identical to the input pump (notice the different scales given in the figure caption). The ring in the far field of the signal has a radius equal to the wave number that becomes critical above threshold. We calculate the correlation of the fluctuations of the signal modes on this critical ring. We chose a signal mode with a given \mathbf{k}_i over the ring, at a time t_i , and calculate the correlation with any other signal mode with wavevector \mathbf{k}_j over the ring, at time t_j . The correlation function g_2 is then a function of the angle between \mathbf{k}_i and \mathbf{k}_j and the time difference $t_d = t_i - t_j$.

In Figure 2 we plot the g_2 output field correlation function against the dimensionless scaled time $\gamma_1 t_d$ and the angle. Note that, as discussed in Section 3, a value of $g_2 = 1$ corresponds to the uncorrelated case and what is relevant is the deviation of g_2 from $g_2 = 1$. There are strong correlations at angles 0 and π which decay exponentially with the time difference and practically no correlation at any other angle. A cut of Figure 2 for zero time difference is shown in Figure 3 where again the 0 and π correlations are seen while for the rest of the angles $g_2 \approx 1$. The correlation at angle 0 corresponds to the signal far field mode self-correlation while the one at angle π corresponds to the

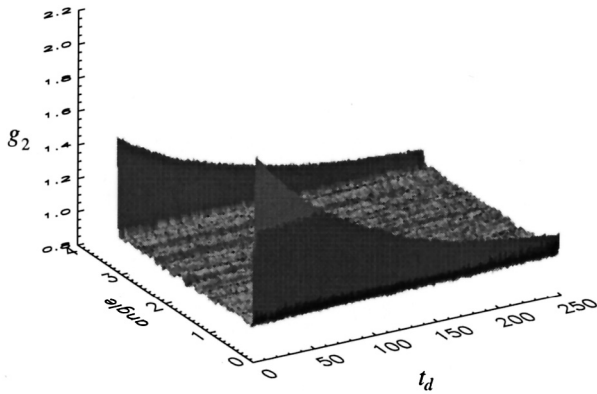


Fig. 2. Correlation function g_2 between two signal modes with critical wave number as function of the time difference t_d and the angle (in radians) between the wave-vectors of the modes. The pump value is just below the threshold for pattern formation $\bar{E}_{\text{in}} = 0.999E_{\text{thr}}$. g_2 has been calculated using 11 400 samples separated a time interval $\gamma_1 \Delta t = 1$ in a lattice of 256×256 points.

correlation between signal modes with opposite wave vector. The correlation at angle π , also visible in the far field of the signal in Figure 1, is also found when a stripe pattern is formed. It can be understood from the linearized equations in a similar way as in [3] and in [10, 27] for a Kerr cavity. Assuming a homogeneous constant pump field E_{in} and linearizing equation (6) around the homogeneous solution (10) we obtain in Fourier space

$$\frac{\partial \alpha_1(\mathbf{k}, t)}{\partial t} = -\gamma_1(1 + i\Delta_1 + ia_1 k^2)\alpha_1(\mathbf{k}, t) + g\alpha_{0,s}\alpha_1^*(-\mathbf{k}, t) + \sqrt{2\gamma_1}\xi_1(\mathbf{k}, t). \quad (20)$$

This equation shows a linear coupling between the amplitude of the signal field $\alpha_1(\mathbf{k})$ with the amplitude with opposite wave-vector $\alpha_1(-\mathbf{k})$. The coupling comes from a term that breaks the phase invariance of the equation for α_1 and its strength is proportional to the homogeneous component of the pump field which always takes a large value. This linear coupling originates strong correlations in the intracavity signal modes with opposite wave-vectors which are the responsables for the output field correlations measured by the function g_2 at angle π . Therefore the origin of the correlations between signal modes with opposite wave-number can be traced back to the symmetry breaking originated by the pump field. The π angle correlations are present both below and above threshold. In the case below threshold, it can be observed even for pump values quite below threshold since the symmetry breaking originated by the pump is always present.

The π -angle correlation can be interpreted as an effect of transverse momentum conservation in the parametric down-conversion process. When a pump photon with frequency 2ω interacts with the nonlinear medium and the parametric down conversion is produced, two signal photons with frequency ω are generated. The two emitted photons have opposite transverse wave-vectors due to momentum conservation.

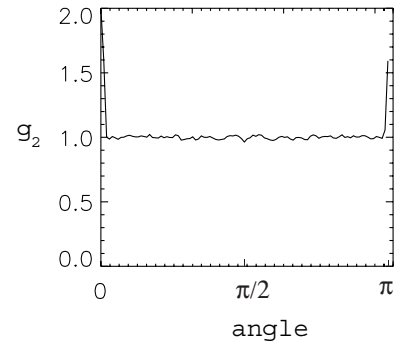


Fig. 3. Transverse cut of Figure 2 at $t = 0$.

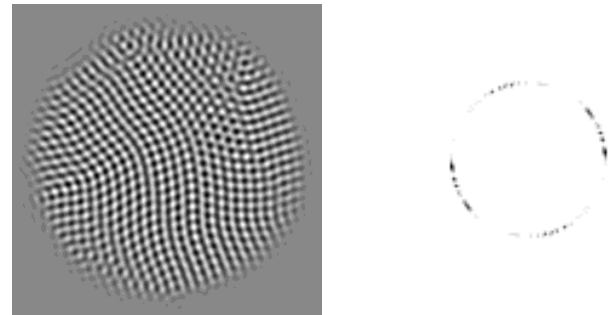


Fig. 4. Snapshot of the signal field configuration above threshold at an intermediate stage starting from random initial conditions ($\gamma_1 t = 2000$, $\bar{E}_{\text{in}} = 1.02\bar{E}_{\text{thr}}$). Left: Real part of the near field $\Re(\alpha_1(\mathbf{x}))$ where the grayscale goes from -0.174 (black) to $+0.174$ (white). Right: far field intensity $|\alpha_1(\mathbf{k})|^2$. As in Figure 1 a lattice of 256×256 points was used.

The square form of the pattern above threshold suggest the presence of correlations between signal modes with wave vectors forming an angle of $\pi/2$. The presence of such correlation below threshold would give us information about the kind of pattern that is formed above threshold. Equation (20) does not show any coupling between the signal modes with wave-vectors forming a $\pi/2$ angle thus indicating that there is no linear coupling between these modes. Therefore below threshold correlations at a $\pi/2$ angle could only come from nonlinear interactions, and therefore could be seen only very close to threshold. The numerical simulations at 0.999 the threshold value do not show any correlation at $\pi/2$ that can be distinguished within our numerical accuracy (see Figs. 2 and 3). Typically this is a value close enough to threshold to see the correlations originated by nonlinear critical fluctuations [27]. We will analyze the $\pi/2$ angle correlations in more detail in Section 5 in the context of a model in which the form of the pattern is assumed *a priori*.

4.2 Results above threshold

For pump values above threshold, starting from random initial conditions a square pattern is formed in the circular region of the transverse plane where the pump is above threshold (Fig. 4). The square pattern arises as a

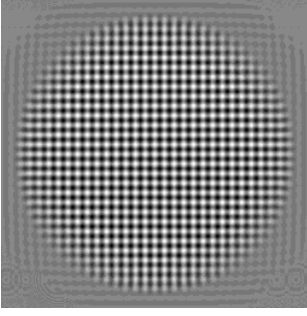


Fig. 5. Final stage of the signal field where a completely ordered square pattern is formed above threshold ($\bar{E}_{\text{in}} = 1.02\bar{E}_{\text{thr}}$). Left: real part of the near field $\Re(\alpha_1(\mathbf{x}))$ (grayscale as in Fig. 4). Right: far field intensity $|\alpha_1(\mathbf{k})|^2$. (A lattice of 256×256 points was used.)

consequence of spontaneous breaking of the radial symmetry, therefore the pattern can be oriented in any direction [25,26]. For a large system and starting from random initial conditions domains with different orientations arise as shown in Figure 4. Over long time scales these domains compete and at the very end one of them will extend through the entire system. Such a pattern is shown in Figure 5, where a square pattern of small amplitude, appropriate wavelength and oriented along the horizontal and vertical directions plus noise was used as initial condition in order to make the system converge to the final stage in a short time. The snapshots show the signal field for a value of the pump of $\bar{E}_{\text{in}} = 4.2 = 1.02\bar{E}_{\text{thr}}$, in the near and far field.

Figure 6 shows the function g_2 for correlations above threshold at angle π (continuous lines) and at angle $\pi/2$ (dashed line). The correlation between opposite modes is again a manifestation of the twin photon emission. The anticorrelation between orthogonal modes is a new effect that we found only above threshold, when the square pattern is already formed. The reason why it is a negative correlation (that in terms of the second-order coherence means $g_2 < 1$) is explained below in Section 5.1.

5 The 4 modes model

Let us consider the system above and close to the threshold for square pattern formation. The signal field is projected onto 4 spatial modes forming a square approximating it by

$$\alpha_1 = A_1 e^{ik_c x} + A_2 e^{-ik_c x} + A_3 e^{ik_c y} + A_4 e^{-ik_c y}, \quad (21)$$

where k_c is the critical wave number of the instability (we have chosen the coordinate axis oriented along the square modes).

Due to the term α_1^2 in equation (5), the modes $(\pm 2k_c, 0)$, $(0, \pm 2k_c)$ and $(\pm k_c, \pm k_c)$ of α_0 will be excited,

so that

$$\begin{aligned} \alpha_0 = & B_0 + B_1 e^{i2k_c x} + B_2 e^{-i2k_c x} + B_3 e^{i2k_c y} + B_4 e^{-i2k_c y} \\ & + B_5 e^{ik_c(x+y)} + B_6 e^{-ik_c(x+y)} + B_7 e^{ik_c(x-y)} \\ & + B_8 e^{-ik_c(x-y)} \end{aligned} \quad (22)$$

with $|B_i| \ll |B_0|$ for $i = 1 \dots 8$. The homogeneous mode B_0 is much larger than the B_i modes because it is related to the input pump field, while the B_i modes are related to the pattern modes A_i that, close to threshold, should be small.

A system of 13 equations is obtained by replacing equations (21, 22) in equations (5, 6). The equations corresponding to the signal modes are

$$\begin{aligned} \frac{dA_1}{dt} = & -\gamma_1(1 + i\Delta_1 + ia_1 k_c^2)A_1 \\ & + g(B_0 A_2^* + B_1 A_1^* + B_5 A_3^* + B_7 A_4^*) + \sqrt{2\gamma_1}\xi_{1,1} \\ \frac{dA_2}{dt} = & -\gamma_1(1 + i\Delta_1 + ia_1 k_c^2)A_2 \\ & + g(B_0 A_1^* + B_2 A_2^* + B_8 A_3^* + B_6 A_4^*) + \sqrt{2\gamma_1}\xi_{1,2} \\ \frac{dA_3}{dt} = & -\gamma_1(1 + i\Delta_1 + ia_1 k_c^2)A_3 \\ & + g(B_0 A_4^* + B_3 A_3^* + B_5 A_1^* + B_8 A_2^*) + \sqrt{2\gamma_1}\xi_{1,3} \\ \frac{dA_4}{dt} = & -\gamma_1(1 + i\Delta_1 + ia_1 k_c^2)A_4 \\ & + g(B_0 A_3^* + B_4 A_4^* + B_6 A_2^* + B_7 A_1^*) + \sqrt{2\gamma_1}\xi_{1,4}. \end{aligned} \quad (23)$$

For the pump modes we have

$$\begin{aligned} \frac{dB_0}{dt} = & -\gamma_0(1 + i\Delta_0)B_0 + E_{\text{in}} - g(A_1 A_2 + A_3 A_4) \\ & + \sqrt{2\gamma_0}\xi_{0,0} \\ \frac{dB_1}{dt} = & -\gamma_0(1 + i\Delta_0 + ia_0 4k_c^2)B_1 - gA_1^2/2 + \sqrt{2\gamma_0}\xi_{0,1} \\ \frac{dB_2}{dt} = & -\gamma_0(1 + i\Delta_0 + ia_0 4k_c^2)B_2 - gA_2^2/2 + \sqrt{2\gamma_0}\xi_{0,2} \\ \frac{dB_3}{dt} = & -\gamma_0(1 + i\Delta_0 + ia_0 4k_c^2)B_3 - gA_3^2/2 + \sqrt{2\gamma_0}\xi_{0,3} \\ \frac{dB_4}{dt} = & -\gamma_0(1 + i\Delta_0 + ia_0 4k_c^2)B_4 - gA_4^2/2 + \sqrt{2\gamma_0}\xi_{0,4} \\ \frac{dB_5}{dt} = & -\gamma_0(1 + i\Delta_0 + ia_0 2k_c^2)B_5 - gA_1 A_3 + \sqrt{2\gamma_0}\xi_{0,5} \\ \frac{dB_6}{dt} = & -\gamma_0(1 + i\Delta_0 + ia_0 2k_c^2)B_6 - gA_2 A_4 + \sqrt{2\gamma_0}\xi_{0,6} \\ \frac{dB_7}{dt} = & -\gamma_0(1 + i\Delta_0 + ia_0 2k_c^2)B_7 - gA_1 A_4 + \sqrt{2\gamma_0}\xi_{0,7} \\ \frac{dB_8}{dt} = & -\gamma_0(1 + i\Delta_0 + ia_0 2k_c^2)B_8 - gA_2 A_3 + \sqrt{2\gamma_0}\xi_{0,8} \end{aligned} \quad (24)$$

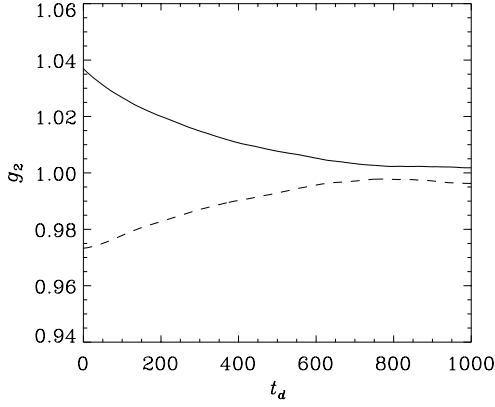


Fig. 6. Correlations above threshold ($\bar{E}_{\text{in}} = 1.02\bar{E}_{\text{thr}}$) obtained from the continuous model. The figure shows the correlation g_2 between two signal modes with critical opposite wave vectors (solid line) and with critical wave vectors forming a $\pi/2$ angle (dashed line) as function of the time difference t_d . To obtain a better statistics, a system of size 64×64 was used. We averaged over 100 000 samples separated a time interval $\gamma_1 \Delta t = 0.5$.

where $\xi_{i,j}$ represent the Gaussian noise terms with correlations

$$\langle \xi_{i,j}(t) \xi_{i',j'}^*(t') \rangle = \frac{1}{2} \frac{1}{L^2} \delta_{i,i'} \delta_{j,j'} \delta(t-t')$$

where L is the transverse size of the system.

Equations (23, 24) are the minimal model to describe square patterns. Note that we can not neglect the second harmonic contributions, B_i ($i = 1..8$), despite its small amplitude in comparison with B_0 , because these modes play an important role in the couplings above threshold. As shown in equation (23) they are responsible for the coupling between signal modes with wave vectors forming a $\pi/2$ angle. Therefore 13 is the minimum number of equations that we need to take into account.

5.1 Correlations above threshold

We first address the correlations above threshold given by the 4 signal modes model. Above (but close to) threshold of square pattern formation there are only four relevant modes for the signal field, as can be seen in Figure 5 therefore this truncated model should reproduce adequately the dynamics of the continuous model. An example of very good agreement between the quantum correlations calculated numerically in a continuous model above threshold and the correlations calculated from the equivalent reduced model can be found in reference [10], that deals with a Kerr medium.

We integrate numerically the nonlinear equations (23, 24), including the noise terms, for a pump value 2% above threshold. Figure 7a shows the the numerical

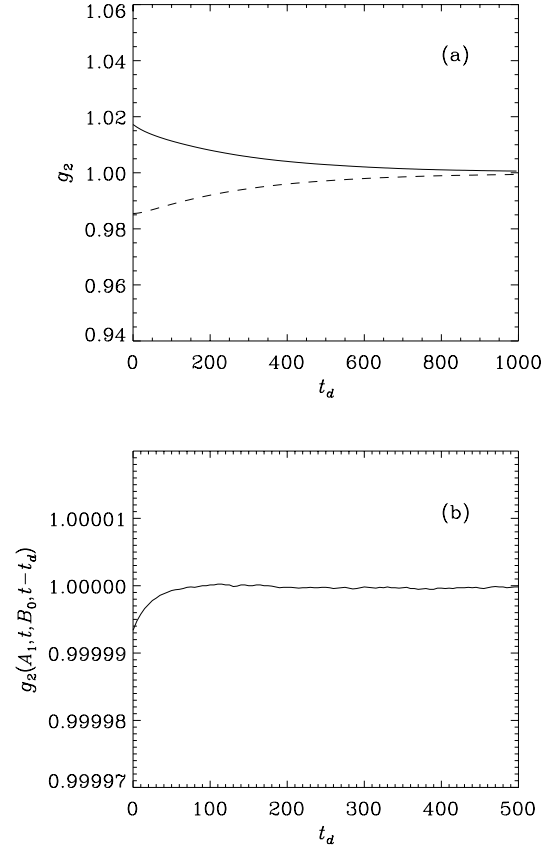


Fig. 7. Correlations above threshold ($\bar{E}_{\text{in}} = 1.02\bar{E}_{\text{thr}}$) obtained from the 4-mode model. Figure (a) shows the correlation g_2 between two signal modes with critical opposite wave vectors (solid line) and with critical wave vectors forming a $\pi/2$ angle (dashed line) as function of the time difference t_d . Figure (b) shows the g_2 correlation function between one of the signal modes, A_1 , and the homogeneous component of the pump field (B_0). g_2 has been calculated using 10^6 samples separated a time interval $\gamma_1 \Delta t = 5$.

results for the correlation function between two signal modes with critical opposite wave vectors and with critical wave vectors forming a $\pi/2$ angle as function of the time difference t_d . There are strong positive correlations at angle π , as obtained from the continuous model which decay exponentially with the time difference. There is also an anticorrelation between the modes with wavevectors forming a $\pi/2$ angle, in agreement with the result obtained for the continuous model.

These correlations can be understood from the linearized equations for the fluctuations around the steady state solution above threshold, $A_{i,s} \neq 0$ and $B_{i,s} \neq 0$, which can be obtained finding the stationary solution of the set of equations (23, 24). This leads to a system of 13 coupled algebraic nonlinear equations that can be solved numerically. Linearizing around this solution we

have for the signal modes

$$\begin{aligned}
\frac{d\delta A_1}{dt} &= -\gamma_1(1 + i\Delta_1 + ia_1k_c^2)\delta A_1 + g(B_{0,s}\delta A_2^* + A_{2,s}^*\delta B_0 \\
&\quad + B_{1,s}\delta A_1^* + A_{1,s}^*\delta B_1 + B_{5,s}\delta A_3^* + A_{3,s}^*\delta B_5 \\
&\quad + B_{7,s}\delta A_4^* + A_{4,s}^*\delta B_7) + \sqrt{2\gamma_1}\xi_{1,1} \\
\frac{d\delta A_2}{dt} &= -\gamma_1(1 + i\Delta_1 + ia_1k_c^2)\delta A_2 + g(B_{0,s}\delta A_1^* + A_{1,s}^*\delta B_0 \\
&\quad + B_{2,s}\delta A_2^* + A_{2,s}^*\delta B_2 + B_{8,s}\delta A_3^* + A_{3,s}^*\delta B_8 \\
&\quad + B_{6,s}\delta A_4^* + A_{4,s}^*\delta B_6) + \sqrt{2\gamma_1}\xi_{1,2} \\
\frac{d\delta A_3}{dt} &= -\gamma_1(1 + i\Delta_1 + ia_1k_c^2)\delta A_3 + g(B_{0,s}\delta A_4^* + A_{4,s}^*\delta B_0 \\
&\quad + B_{3,s}\delta A_3^* + A_{3,s}^*\delta B_3 + B_{5,s}\delta A_1^* + A_{1,s}^*\delta B_5 \\
&\quad + B_{8,s}\delta A_2^* + A_{2,s}^*\delta B_8) + \sqrt{2\gamma_1}\xi_{1,3} \\
\frac{d\delta A_4}{dt} &= -\gamma_1(1 + i\Delta_1 + ia_1k_c^2)\delta A_4 + g(B_{0,s}\delta A_3^* + A_{3,s}^*\delta B_0 \\
&\quad + B_{4,s}\delta A_4^* + A_{4,s}^*\delta B_4 + B_{6,s}\delta A_2^* + A_{2,s}^*\delta B_6 \\
&\quad + B_{7,s}\delta A_1^* + A_{1,s}^*\delta B_7) + \sqrt{2\gamma_1}\xi_{1,4}. \quad (25)
\end{aligned}$$

This set of equations shows a linear coupling between the fluctuations of modes separated by an angle π , such as δA_1 and δA_2 or δA_3 and δA_4 , and by an angle $\pi/2$ such as for example between δA_1 and δA_3 or δA_4 . In the first case the strength of the coupling is proportional to the homogeneous component of the intracavity pump field $B_{0,s}$ while the $\pi/2$ angle coupling is mediated by the stationary values of the pump field pattern modes $B_{i,s}$ ($i = 1 \dots 8$). This linear coupling will imply significantly large correlations between the signal output field modes with wave vectors forming a π and a $\pi/2$ angle as obtained numerically from the nonlinear equations (23, 24) and shown in Figure 7.

An alternative way to explain the correlation above threshold between the output signal far field modes forming an angle $\pi/2$ can be obtained from the energy expression we derived at the end of Section 2. As above threshold the square pattern is fully developed, we can approximate $|A_1| \simeq |A_2|$ and $|A_3| \simeq |A_4|$, so

$$\alpha_1 = A_1 \cos(k_c x + \phi_x) + A_3 \cos(k_c y + \phi_y). \quad (26)$$

Replacing equations (26, 22) in equation (12), we get

$$P = 2\hbar\omega L^2 [2\Re(E_{\text{in}}B_0^*) - 2\gamma_0|B_0|^2 - \gamma_1(|A_1|^2 + |A_3|^2)], \quad (27)$$

where L is the transverse size of the system, and we have neglected terms of order $B_i B_j$ with $i, j = 1 \dots 8$. Since in a steady state P have small fluctuations around zero, the fluctuations of the quantities in the r.h.s. of equation (27) must cancel. For example, a positive fluctuation of $|A_1|^2$ can be compensated by a negative fluctuation of $|A_3|^2$.

We have also calculated the correlation function g_2 at the output between a mode of the signal (A_1) and the homogeneous mode of the pump (B_0), that we call $g_2(A_1, t, B_0, t')$. As shown in Figure 7 there is a small anticorrelation at equal times which quickly decays as the

time difference increases. The linearized equations (25) show also a coupling between δA_1 and δB_0 with a strength proportional to $A_{2,s}^*$ which can be considered the responsible for this anticorrelation. Likewise, this anticorrelation can be understood from equation (27).

The anticorrelations above threshold between orthogonal signal modes and between signal modes and pump mode can be explained in terms of the possible photon processes in the parametric down conversion. Let us consider the system above threshold with a perfectly ordered square pattern. When a pump photon with frequency 2ω enters the cavity there can be mainly three processes: (i) the photon leaves the cavity without interacting with the medium. (ii) The photon interacts with the medium *via* a parametric down conversion and two photons of frequency ω leave the cavity and produce two spots in the horizontal direction in the far field. (iii) Same as (ii) but the two photons that leave the cavity are emitted in the vertical direction. There are more complicated processes, but we can neglect their relevance with respect to the three mentioned. Each process has a probability to occur that is proportional to the intensity of the spots in the far field. Let us suppose that, for example, process (i) takes place. Then, the photon gives all its energy to the homogeneous pump mode, and nothing to the four signal modes. This represents a positive fluctuation of the homogeneous pump mode with respect to the average intensity, and a negative fluctuation of the signal modes, giving rise to an anticorrelation between signal and pump, as is seen in Figure 7b (this argument holds also below threshold, where the signal modes form the critical circle). If, instead, process (ii) takes place, the input photon gives all its energy to the horizontal signal modes. There is a positive fluctuation of the horizontal signal modes and a negative fluctuation of the vertical signal modes and the homogeneous pump mode with respect to the average intensity. Then, an anticorrelation between horizontal and vertical signal modes will take place, as seen in the plot of the correlation at angle $\pi/2$ in Figures 6 and 7a. Analogous result is obtained for process (iii).

The above arguments identify the origin of anticorrelations, however, they do not imply that these anticorrelations are below a shot noise level. Therefore one has to rely on the calculation to determine if the suggested anticorrelations are in fact at a quantum level or not.

5.2 Correlations below threshold

We now address the question of the correlations just below threshold ($\bar{E}_{\text{in}} = 4.119 = 0.999\bar{E}_{\text{thr}}$) given by the 4 modes model (23, 24). Although the 4-modes model is a good approximation of the continuous model only above and close to threshold, we explore its use to calculate the correlations below threshold. The problem below threshold is that this simplified model represents a truncated version of the continuous model, where the infinite number of modes in the critical circle of the signal far field is reduced to 4.

Figure 8a shows the numerical results for the correlation function between two signal modes with critical opposite wave vectors and with critical wave vectors forming a $\pi/2$ angle as function of the time difference t_d . As in the case above threshold, there are strong positive correlations at angle π , as obtained from the continuous model, which decay exponentially with the time difference. The new result is that there is also an anticorrelation between the modes with wavevectors forming a $\pi/2$ angle.

The steady state solution below threshold is $A_{i,s} = 0$ ($i = 1..4$), $B_{i,s} = 0$ ($i = 1..8$), and only $B_{0,s}$ is different from zero. If we linearize around this solution we get, for the signal modes

$$\begin{aligned} \frac{d\delta A_1}{dt} &= -\gamma_1(1 + i\Delta_1 + ia_1k_c^2)\delta A_1 + gB_{0,s}\delta A_2^* + \sqrt{2\gamma_1}\xi_{1,1} \\ \frac{d\delta A_2}{dt} &= -\gamma_1(1 + i\Delta_1 + ia_1k_c^2)\delta A_2 + gB_{0,s}\delta A_1^* + \sqrt{2\gamma_1}\xi_{1,2} \\ \frac{d\delta A_3}{dt} &= -\gamma_1(1 + i\Delta_1 + ia_1k_c^2)\delta A_3 + gB_{0,s}\delta A_4^* + \sqrt{2\gamma_1}\xi_{1,3} \\ \frac{d\delta A_4}{dt} &= -\gamma_1(1 + i\Delta_1 + ia_1k_c^2)\delta A_4 + gB_{0,s}\delta A_3^* + \sqrt{2\gamma_1}\xi_{1,4}, \end{aligned} \quad (28)$$

which shows the presence of linear couplings between the amplitude of the fluctuations of modes with opposite wave vectors: δA_1 and δA_2 or δA_3 and δA_4 . As in the linearized continuous model (20) discussed in the previous section, the strength of the coupling is proportional to the homogeneous mode $B_{0,s}$ which is always strong. This linear coupling is responsible for the strong correlation found in the g_2 function between output signal modes with opposite wave vector. Also, as in the continuous model there is no coupling, in the linearized equations, between the fluctuations of signal modes with wave vectors forming a $\pi/2$ angle. Above threshold this coupling was proportional to the amplitude of the pump pattern modes, which is zero below threshold. The $\pi/2$ angle correlations come from nonlinear interactions, and therefore can be seen only very close to threshold. In fact we see them here because we are just at 0.1% below threshold. This result is due to the mode-truncation and disappears moving further below threshold and in the continuous limit. For example, if we consider an input field of $\bar{E}_{\text{in}} = 0.9\bar{E}_{\text{thr}}$, the correlations at angle π remain strong while the nonlinear correlations at $\pi/2$ vanish as shown in Figure 9a.

Finally we show in Figure 8 the correlation $g_2(A_1, t, B_0, t')$ between the A_1 mode of the signal, and the homogeneous pump mode B_0 . As in the case above threshold there is a small anticorrelation at equal times which quickly decays as the time difference increases. Again there is no coupling in the linearized equations (28) between the signal mode and the pump mode fluctuations, so this correlation comes from nonlinear interactions and it can be observed only very close to threshold. As shown in Figure 9 this correlation vanishes for pump $\bar{E}_{\text{in}} = 0.9\bar{E}_{\text{thr}}$.

A final remark is that the correlations measured through the function g_2 just below threshold, can be stronger than the ones above threshold (compare Fig. 8 with Fig. 7). This occurs even in the case of the $\pi/2$ corre-

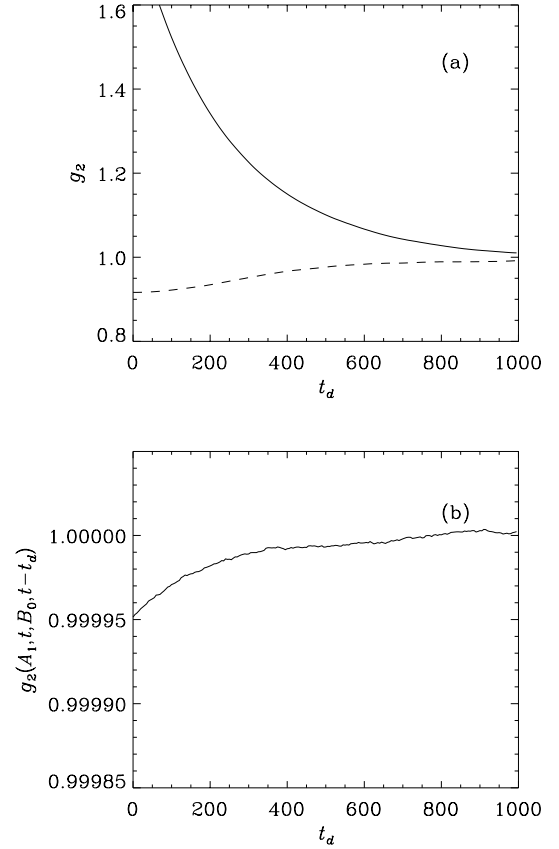


Fig. 8. Correlations just below threshold $\bar{E}_{\text{in}} = 0.999\bar{E}_{\text{thr}}$ obtained from the 4-mode model. The upper figure shows the correlation g_2 between two signal modes with critical opposite wave vectors (solid line) and with critical wave vectors forming a $\pi/2$ angle (dashed line) as function of the time difference t_d . The lower figure shows the g_2 correlation function between one of the signal modes, A_1 , and the homogeneous component of the pump field (B_0). g_2 has been calculated using 10^6 samples separated a time interval $\gamma_1\Delta t = 5$.

lation which just below threshold appears only due to nonlinear effects while above threshold is generated by linear couplings. This result can be understood taking into account the fact that the g_2 function is normalized with the mode intensities and the average intensity of the modes just below threshold is much smaller than above it.

6 Final discussion and conclusion

We found three types of quantum correlations close to an instability for square pattern formation in degenerate optical parametric oscillators. First, a strong correlation between opposite wave-vector modes of the signal far field. It is clearly present in both the continuous and the 4 modes model and it can be understood as an effect of momentum conservation in the parametric down conversion process of one pump photon into two signal photons (twin photon emission). Alternatively its origin can be related to the phase symmetry breaking induced by the pump field similar to what is obtained for a Kerr cavity [27]. The coupling

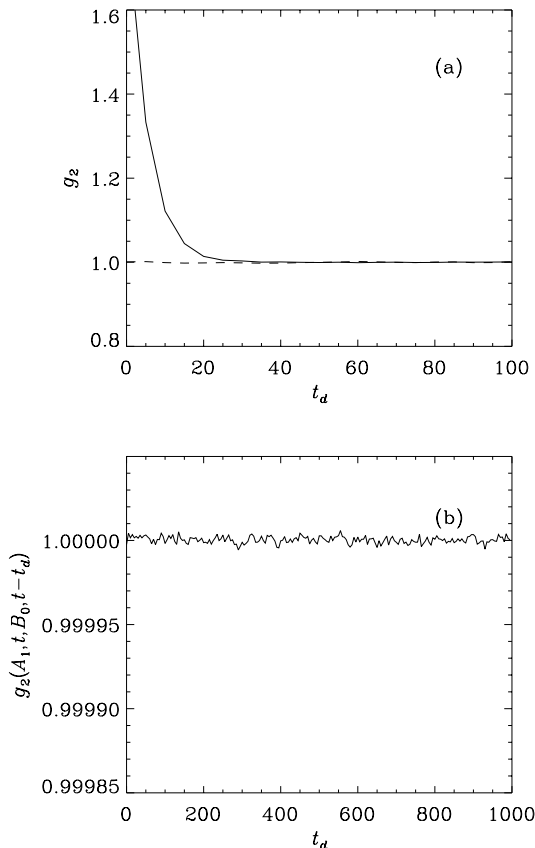


Fig. 9. The same correlations obtained from the 4-mode model as in Figure 8 but for $\bar{E}_{\text{in}} = 0.9\bar{E}_{\text{thr}}$.

between opposite wave-vector signal modes already appears in the linearized equations around the steady state, both below and above threshold and therefore this correlation appear either above or below threshold, and not necessarily close to it. Quantum aspects of this correlation were already studied, specially in the case of a stripe pattern formation [3, 4, 28], and more recently in spatially disordered structures [18].

Second, above threshold, we find anticorrelation between the signal field modes with critical wave vectors forming an angle of $\pi/2$. This correlation can be explained from the linearized equations above threshold which show a direct coupling between the fluctuations of these modes. Below threshold the amplitude of the pump field pattern modes is zero and therefore in the linearized equations there is no coupling between the fluctuations of the signal modes with wave vectors forming a $\pi/2$ angle. In fact, pattern selection is a nonlinear process, and the question of which pattern is selected cannot be answered by a linear analysis. Despite that, using the nonlinear 4 modes model, one finds correlations between these modes for pump values extremely close to threshold ($\bar{E}_{\text{in}} = 0.999\bar{E}_{\text{thr}}$) which come from the nonlinearities and are a manifestation of critical fluctuations. These correlations quickly vanishes decreasing the pump value. In the continuous model, how-

ever, we found numerically no correlations between the signal modes emitted with wave vectors forming a $\pi/2$ angle even extremely close to threshold ($\bar{E}_{\text{in}} = 0.999\bar{E}_{\text{thr}}$). The statistics we have for the continuous model involve 11 400 samples and therefore the numerical result for the g_2 correlation has a limited precision. The result we obtain for the correlation function g_2 differs from 1.00 (uncorrelated case) in less than 0.03 which is within the limits of the statistics. This is significantly different from the value $g_2 = 0.92$ obtained from the 4 mode model at the same pump level. We believe that the $\pi/2$ correlations obtained from the 4 mode model are over-magnified by the reduction of the number of critical modes to 4 in the signal field instead of considering the continuous ring of critical modes $|\mathbf{k}| = k_c$. Therefore, we can not say that the correlations between the fluctuations below threshold do carry any information about the specific square form of the pattern that arises above threshold. They are a noisy precursor of the pattern in the sense that they tell us about the critical wave number of the pattern but they are not a quantum image of the pattern that shows what kind of pattern is formed above threshold.

We also find an anticorrelation between the homogeneous pump mode and any of the critical signal modes. Numerical results of the 4-modes model shows that it is present above or below threshold. A similar anticorrelation has been found in a Kerr medium [27]. Above threshold this anticorrelation comes from linear coupling in the linearized equations. Below threshold it is a manifestation of non-linear critical fluctuations, and therefore it can be observed only very close to threshold.

We want to stress that the analysis of the correlations in terms of the linear couplings has the purpose of identifying which correlations have a linear origin, but all the numerical results have been obtained with the full nonlinear equations.

Finally, we note that our results are based on the numerical evaluation of the second-order coherence function g_2 . The use of this function in the characterization of quantum properties of spatially extended nonlinear optical systems is far more general than the specific case of square patterns studied here. The evaluation of the g_2 function and a comparison with experimental result can be beneficial when studying, for example, quantum correlations between fluctuations around spatially localized features such as domain walls and dark ring cavity solitons [23].

We want to acknowledge essential discussions for the accomplishment of this work with S.M. Barnett, A. Gatti and L.A. Lugiato. This work is supported by the European Commission through the TMR network QSTRUCT (FMRX-CT96-0077) and through the project QUANTIM (IST-2000-26019) and from the MCyT (Spain, Projects PB97-0141-C02-02 and BFM2000-1108). M.H. wants to acknowledge financial support from CONICET grant PIP NO.4342, and Fundaci3n Antorchas, Argentina. G-LO acknowledges SGI and EPSRC for financial support.

Appendix A: Numerical calculation of α_i^{out}

The space-time evolution of α_0^{out} and α_1^{out} can be obtained numerically using the method presented in [10]. We write equations (5, 6) for the intracavity fields as, $\partial_t \alpha_i = f_i(\alpha_0, \alpha_1) + \sqrt{2\gamma_i} \xi_i$, where the index i is 0 or 1. We consider a discretized time $t = n\tau$, where τ is a small time step and n is an integer. At time $n\tau + s$ we have

$$\alpha_i(n\tau + s) \simeq \alpha_i(n\tau) + f_i(n\tau) s + \sqrt{2\gamma_i} \int_{n\tau}^{n\tau+s} \xi_i(t) dt. \quad (\text{A.1})$$

The average value of α_i in the time interval $n\tau \rightarrow n\tau + \tau$ is

$$\begin{aligned} \alpha_{i,n} &= \frac{1}{\tau} \int_0^\tau \alpha_i(n\tau + s) ds \\ &\simeq \alpha_i(n\tau) + f_i(n\tau) \frac{\tau}{2} + \frac{\sqrt{2\gamma_i}}{\tau} \int_0^\tau ds \int_{n\tau}^{n\tau+s} \xi_i(t) dt \\ &\simeq \frac{\alpha_i(n\tau) + \alpha_i(n\tau + \tau)}{2} - \sqrt{\frac{\gamma_i}{2}} \int_{n\tau}^{n\tau+\tau} \xi_i(t) dt \\ &\quad + \frac{\sqrt{2\gamma_i}}{\tau} \int_0^\tau ds \int_{n\tau}^{n\tau+s} \xi_i(t) dt. \end{aligned} \quad (\text{A.2})$$

The space dependence is not explicitly written to simplify the notation. Using the input-output relation $\alpha_i^{\text{out}} = \sqrt{2\gamma_i} \alpha_i - (\mathcal{E}_i + \xi_i)$, where $\mathcal{E}_0 = E_{\text{in}}/\sqrt{2\gamma_0}$ and $\mathcal{E}_1 = 0$, and equation (A.2) we get the average value of the output field at time step $n\tau$

$$\begin{aligned} \alpha_{i,n}^{\text{out}} &= \frac{1}{\tau} \int_0^\tau \alpha_i^{\text{out}}(n\tau + s) ds \\ &= \sqrt{2\gamma_i} \frac{\alpha_i(n\tau) + \alpha_i(n\tau + \tau)}{2} - \mathcal{E}_i + \zeta_{i,n} \end{aligned} \quad (\text{A.3})$$

where $\zeta_{i,n}$ is the noise of the output field at time step $n\tau$; it is related to the input noise ξ_i via the equation

$$\begin{aligned} \zeta_{i,n} &= \frac{2\gamma_i}{\tau} \int_0^\tau ds \int_{n\tau}^{n\tau+s} \xi_i(s') ds' \\ &\quad - \frac{1 + \gamma_i \tau}{\tau} \int_{n\tau}^{n\tau+\tau} \xi_i(s) ds. \end{aligned} \quad (\text{A.4})$$

The previous equations hold for both near field and far field, since they are linear. The correlations of ζ_i , in the far field, are

$$\langle \zeta_{i,n}(\mathbf{k}) \zeta_{i,n'}^*(\mathbf{k}') \rangle = \frac{1}{2\tau} \left(\frac{\gamma_i^2 \tau^2}{3} + 1 \right) \delta_{nn'} \delta(\mathbf{k} - \mathbf{k}') \quad (\text{A.5})$$

$$\langle \zeta_{i,n}(\mathbf{k}) \xi_{i,n'}^*(\mathbf{k}') \rangle = -\frac{1}{2\tau} \delta_{nn'} \delta(\mathbf{k} - \mathbf{k}') \quad (\text{A.6})$$

where $\xi_{i,n}(\mathbf{k}) = (1/\tau) \int_{n\tau}^{n\tau+\tau} \xi_i(\mathbf{k}, t) dt$. The correlations are fulfilled if we relate $\zeta_{i,n}$ to $\xi_{i,n}$ as

$$\zeta_{i,n}(\mathbf{k}) = -\xi_{i,n}(\mathbf{k}) + \frac{\gamma_i \tau}{\sqrt{3}} \sigma_n(\mathbf{k}) \quad (\text{A.7})$$

where $\sigma_n(\mathbf{k})$ is a Gaussian noise with $\langle \sigma_n(\mathbf{k}) \sigma_{n'}^*(\mathbf{k}') \rangle = (1/2\tau) \delta_{nn'} \delta(\mathbf{k} - \mathbf{k}')$.

In the numerical simulations we used τ equal to the time step of the integration scheme.

References

1. A. Gatti, L.A. Lugiato, Phys. Rev. A **52**, 1675 (1995)
2. L.A. Lugiato, I. Marzoli, Phys. Rev. A **52**, 4886 (1995)
3. A. Gatti, H. Wiedemann, L.A. Lugiato, I. Marzoli, G.-L. Oppo, S.M. Barnett, Phys. Rev. A **56**, 877 (1997); A. Gatti, L.A. Lugiato, G.-L. Oppo, R. Martin, P. Di Trapani, A. Berzanskis, Opt. Expr. **1**, 21 (1997)
4. L.A. Lugiato, A. Gatti, H. Ritsch, I. Marzoli, G.-L. Oppo, J. Mod. Opt. **44**, 1899 (1997)
5. L.A. Lugiato, F. Castelli, Phys. Rev. Lett. **68**, 3284 (1992)
6. L.A. Lugiato, G. Grynberg, Eur. Phys. Lett. **29**, 675 (1995)
7. G. Grynberg, L.A. Lugiato, Opt. Commun. **101**, 69 (1993)
8. J. Jeffers, G.-L. Oppo, Phys. Rev. A **60**, 2393 (1999)
9. C. Szewaj, G.-L. Oppo, A. Gatti, L.A. Lugiato, Eur. Phys. J. D **10**, 433 (2000)
10. R. Zambrini, M. Hoyuelos, A. Gatti, P. Colet, L. Lugiato, M. San Miguel, Phys. Rev. A **62**, 801 (2000)
11. R. Zambrini, S.M. Barnett, P. Colet, M. San Miguel, Phys. Rev. A **65**, 023813 (2002)
12. R. Zambrini, M. San Miguel, Phys. Rev. A **66**, 023807 (2002)
13. M. Bache, P. Scotto, R. Zambrini, M. San Miguel, M. Saffman, Phys. Rev. A **66**, 013809 (2002)
14. P. Lodahl, M. Saffman, Opt. Lett. **27**, 110 (2002)
15. L.A. Lugiato, M. Brambilla, A. Gatti, Adv. At. Mol. Opt. Phys. **40**, 229 (1999)
16. K. Wiesenfeld, J. Stat. Phys. **38**, 1071 (1985)
17. G.-L. Oppo, M. Brambilla, L.A. Lugiato, Phys. Rev. A **49**, 2028 (1994)
18. R. Zambrini, S.M. Barnett, P. Colet, M. San Miguel, Eur. Phys. J. D **22**, 461 (2003)
19. M. Le Berre, E. Ressayre, A. Tallet, J. Opt. B **1**, 107 (1999)
20. S. Longhi, G.-L. Oppo, W.J. Firth, unpublished
21. Alternative approaches to the study of quantum properties of patterns in OPO in terms of Langevin equations are based on the use of the Q representation [18] or a time dependent parametric approximation [11,12]
22. D.F. Walls, G.J. Milburn, *Quantum Optics* (Springer-Verlag, Berlin, 1994)
23. G.-L. Oppo, A.J. Scroggie, W.J. Firth, J. Opt. B **1**, 133 (1999); Phys. Rev. E **63**, 066209 (2001)
24. The operators \hat{a}_i have to be distinguished from the characteristic areas a_0 and a_1
25. M.C. Cross, P.C. Hohenberg, Rev. Mod. Phys. **65**, 851 (1993)
26. D. Walgraef, *Spatio-Temporal Pattern Formation* (Springer-Verlag, New York, 1996)
27. M. Hoyuelos, P. Colet, M. San Miguel, Phys. Rev. E **58**, 74 (1998)
28. I. Marzoli, A. Gatti, L.A. Lugiato, Phys. Rev. Lett. **78**, 2092 (1997)